ELSEVIER

X-ray computed laminography: A brief review of mechanisms, reconstruction, applications and perspectives

Wenjia Du [a,b,c], Francesco Iacoviello [d], Mateen Mirza [d], Shangwei Zhou [d], Junfu Bu [c,e], Shikang Feng [e], Patrick S. Grant [c,e], Rhodri Jervis [c,d], Dan J.L. Brett [c,d], Paul R. Shearing [a,b,c,*]

[a] Department of Engineering Science, University of Oxford, Oxford OX1 3PJ, the United Kingdom of Great Britain and Northern Ireland
[b] The ZERO Institute, University of Oxford, Oxford OX2 0ES, the United Kingdom of Great Britain and Northern Ireland
[c] The Faraday Institution, Quad One, Harwell Science and Innovation Campus, Didcot OX11 0RA, the United Kingdom of Great Britain and Northern Ireland
[d] Electrochemical Innovation Lab, Department of Chemical Engineering, University College London, London WC1E 7JE, the United Kingdom of Great Britain and Northern Ireland
[e] Department of Materials, University of Oxford, Oxford OX1 3PH, the United Kingdom of Great Britain and Northern Ireland

X-ray computed tomography (CT) has the capacity to reveal the internal details of objects in three-dimensions, non-destructively. Since the 1980s, X-ray CT has been accepted as a well-established tool for a wide range of scientific and engineering research endeavours. The sample is rotated about an axis perpendicular to the incident X-ray beam during CT acquisition. The spatial resolution of CT scans may be compromised for large, flat (high-aspect-ratio) samples due to constraints imposed by the geometrical setting. The recent development of X-ray computed laminography (CL) offers a great opportunity to overcome several limitations by using an angled axis of rotation, which could complement CT characterisation. Like X-ray CT, CL is also capable of acquiring 3D image datasets for the extraction of volumetric parameters, such as phase fractions and damage levels. Herein, we review the research on X-ray CL over the past three decades and the current state of the field, including its advantages and disadvantages, characteristics, methods and setup, data reconstruction and computational software, and applications. Finally, the outlook for future research opportunities and challenges is briefly discussed. The preliminary attempts to implement CL for electrochemical devices are presented with a focus on research pertaining to pilot-scale solid-state pouch batteries.

Keyword: X-ray Computed Laminography

Introduction

X-ray computed tomography (CT) is a characterisation technique for providing a comprehensive overview of the internal as well as the external structure of materials non-destructively, with spatial resolutions ranging from the centimetres (macroscale) down to the tens of nanometre scale (nanoscale) [1]. This tool can generate a series of 2D radiographs of a given object from all directions around a rotational axis with the final output referred to as a CT scan. A computed reconstruction algorithm (commonly a filtered back projection) is then employed to create a stack of cross-sectional slices from these 2D radiographic projections. The obtained greyscale images can be quantitatively analysed and virtually sliced in any direction or can be digitally colour-coded to highlight certain features and subsequently rendered to visualise the 3D morphology.

Since the epochal discovery of X-rays in 1895 by W.C. Röntgen, X-rays have been used primarily in scientific and engineer-

* Corresponding author.
E-mail address: Shearing, P.R. (paul.shearing@eng.ox.ac.uk)

https://doi.org/10.1016/j.mattod.2025.02.023

ing applications from a wide range of subject areas such as materials science, metrology, medicine, biology, palaeontology, and even for purposes of geological exploration [2–4]. Aided by the development of X-ray sources and detector systems, X-ray CT enables the characterisation of samples with sizes ranging from tens of nanometres to metres. Nowadays, X-ray specialists need to perform some critical steps such as image acquisition, reconstruction, and segmentation to visualise samples as 3D images with quantitative analysis. There are numerous tools available for digital image analysis (Table 1), which will be discussed later.

It is straightforward to take CT scans for cylindrical or rotationally symmetric samples. Whereas samples which are flat or those with a high-aspect-ratio and/or irregular geometries, X-ray CT may prove ineffective in obtaining images due to the weaker signal, concomitant noise, and image artefacts. This is because the penetrating power of X-rays is much weaker on the longer side while the much shorter side is overexposed. Also, when a small volume of interest in the middle of a large flat sample that needs to be inspected (so-called 'interior tomography'), conventional X-ray CT relied on geometrical magnification often has limitations in terms of spatial resolution because the axis of rotation of the item under investigation is at 90° to the X-ray beam. Consequently, it is not feasible to position the specimen closer to the X-ray source to increase the magnification of the area of interest and improve resolution, because the sample, as it turns, would collide with the source. As a solution to mitigate the resolution limitation caused by sample size, the use of 3D X-ray microscopes could be beneficial for some cases (without the need for physical proximity to the source) which includes geometric and optical magnification with 'resolution-at-a-distance' (RaaD) capability [4,5].

As another viable solution, X-ray CL image acquisition using tilted X-ray CT setting avoids the spatial limitation (geometrical obstruction) by allowing the axis of rotation to be adjusted to a certain angle, meaning the flat sample can fully rotate beneath the X-ray source (an illustrative animation can be found in Fig. 2 and https://industry.nikon.com/en-gb/products/x-ray-ct/tilted-ct/). Hence, higher magnification with enhanced image resolution can be achieved in faster scan times. It also enhances quality control by producing better signal-to-noise ratio (SNR) of samples of any shape in which dense areas can mask those that are less dense. Another advantage of the CL technique is to eliminate artefacts caused by high-density features/phases in sample obscuring areas where X-ray attenuation is lower. By tilting the axis of rotation, areas of high attenuation can be positioned so that they rotate beneath or above a lower-density area of interest, rather than in front of it. Despite aforementioned advantages, some disadvantages for CL should be considered, as CL has limited depth resolution along the vertical axis, with the artefacts and blurring along the normal axis of the flat plane of the sample.

In comparison to X-ray CT technology, X-ray CL is a technique which remains in a subcategory of the X-ray CT family and is still in its early stages of development [6]. This is mainly due to hardware limitations and the lack of sophisticated software to reconstruct the data. Initial laminographic experiments were conducted in the 1930s by Des Plantes [7], which the detector and X-ray source were moved simultaneously in the opposite direction and sample did not move at all. This tool was then used in medical diagnoses [8]. For conventional CT studies, the object must be illuminated from all directions. CL, on the other hand, is able to overcome such difficulties in the study of flat samples [9].

There are several reasons motivating this work; Li-ion pouch cells are among the most used cell types for EVs due to their cost-effective manufacturing and higher gravimetric energy density. However, the high-aspect-ratio inherent to the pouch geometry poses significant challenges to CT characterisation, which hinders the development of high-performance batteries under authentic conditions. We have recognised that X-ray CL approach could be a valuable tool to overcome limitations and help obtain the internal structure of large-sized samples (up to tens of centimetres). Furthermore, we aim to increase awareness of the CL technique (by giving a few case studies) and attract attentions to its development and use in emerging research. We also envisage that the development of AI technology as a complementary tool may generate greater impact in future CL studies.

Here, a brief review of X-ray CT/CL and synchrotron radiation (SR)-CT/CL technologies is given, including the history, working

TABLE 1

Commonly used software for digital image processing. OA refers to open-access and L refers to licenced which users must subscribe to before use.

Software	Reconstruction	Segmentation	Visualisation	Machine (Deep) Learning	Simulation	Availability
CIL	✓	—	—	—	—	OA
Astra Toolbox	✓	—	—	—	—	OA
Nikon CT Pro	✓	—	—	—	—	L
Tofu	✓	—	—	—	—	OA
ZEISS XMReconstructor gen. 1	✓	—	—	—	—	L
ZEISS XMReconstructor gen. 2 (DeepRecon & DeepScout)	✓	—	—	✓	—	L
ImageJ & Fiji	—	✓	✓	✓	—	OA
SuRVoS	—	✓	✓	✓	—	OA
3D Slicer (Segment Anything Model)	—	✓	✓	✓	✓	OA
Avizo 3D	—	✓	✓	✓	✓	L
VGstudio max	—	✓	✓	—	—	L
Dragonfly	✓	✓	✓	✓	✓	L
Tomviz	—	—	✓	—	—	OA
Matlab	✓	✓	✓	✓	✓	L

principles, data reconstruction, and potential applications. Furthermore, we present the most recent research findings on the application of laboratory X-ray CL for a dense solid-state battery (SSB) pouch. We show it is possible to scan the solid electrolyte layer in its entirety by tilting the pouch so that the sample rotates at the same angle as the X-ray cone beam, effectively eliminating the obstruction. The CL technique provides a viable solution when examining flat, high-aspect-ratio sample, such as pouch batteries.

Theory of X-ray CL

X-ray CL is also known as 'tilted CT' and is an advancement from classical laminography which is based on the principle that the X-ray source and detector move in opposite directions synchronously [9]. CL differs from classical laminography as both the X-ray source and detector remain stationary which enables the visualisation of objects. It has been confirmed that the CL technique can introduce considerable improvements compared to classical laminography [9,11]. The major difference between CT and CL is that the rotating axis of CL is 'tilted' by an angle between 0 and 90° (Fig. 2). There have been studies on the optimisation of the tilted angle for better image quality [16,17]; however, most of the literature adopts tilted angles which are less than 40°.

When one scans a large flat (high-aspect-ratio) object in the laboratory, it is almost impossible to obtain useful CT images since the X-rays cannot penetrate through the extended (longer) side. As a result, the imaging information will either be lost or no suitable information will be acquired from the scan. It should be made clear that while raw X-ray projections with missing information at certain angles can still be reconstructed in principal, the reconstructed CT data generally proves to be less informative [18]. This is because the deleterious artefacts can lead to deterioration in image quality (i.e., signal-to-noise ratio and contrast) which affects subsequent imaging analysis.

In contrast, X-ray penetration will benefit if the planar surface of a large, flat sample is attached to a pre-programmed tilted sample stage. This tilting of the rotational axis means that similar X-ray transmissions through the flat sample can be obtained at all projections (angles). The motion is simplified as there is only one moving part (simply rotate); With the source-detector position remaining constant and their positions are fixed, the geometry has less variations and the beam penetrates through the sample at an angle to the axis of rotation. In particular, the tilted setup increases the overall field of view (FOV) of the charge coupled device (CCD) system. This allows a larger object to be scanned by CL and can reduces or eliminate the need for sample cutting (i.e., by a laser preparation).

To date, there are approximately 260 peer-reviewed articles with regard to CL instrument development, data reconstruction, and CL application (Fig. 1), which demonstrates comparative statistics on related CT and CL research publications in the last two decades. The search for CL was conducted on the Clarivate (Web of Science) using the keywords including 'X-ray computed laminography', 'X-ray laminography', and 'laminography'. It should be noticed that different terminological names such as fluoroscopy and tomosynthesis were once used to refer CL technique, and they are very minority. Similarly, X-ray computed tomography', 'X-ray tomography', and 'tomography' were used to search for the number of CT publications. This figure is unsurprising given the associated restraints with both hardware (complex setup and adjustment compared with CT) and software (available reconstruction algorithms and computational sources) challenges. Like CT, the spatial resolution of common CL can range from the sub-micron to millimetre scale according to the object size and X-ray capability. With the advancement of CL technology, it is expected that both spatial and temporal resolutions will be further improved for wider applications in both academic and industrial settings [19].

Lab and synchrotron X-ray CT/CL

Like CT, CL can also be performed either in the laboratory using a compact source or large-scale facilities using synchrotron radiation (SR) (Fig. 2). Table 2 is summarised to show instrument and national facilities that can be used for CL measurements with identified reference. In comparison with limited-angle SR-CT (i.e., where the angular range from 0 to 180° is accessible), SR-CL scanning protocol maximises the coverage in the Fourier domain, which offers reconstructed images with less disruptive artefacts than SR-CT [17]. One example of this is where Sassov and Luypaert [12] employed a lab-based CL scanner in the year 2000 (when it became commercially available) to inspect two structures of flip-chip and ball grid array (BGA), achieving resolutions between 10–20 μm. In 2005, Helfen et al. [13] developed the first microscale CL system (resolution down to 1 μm) with synchrotron capability at the ID19 beamline in European Synchrotron Radiation Facility (ESRF) (Grenoble, France). The laminography in ID19 was co-developed by Karlsruhe Institute of Technology (KIT) and ESRF. A similar technology was developed by Hoshino et al. [20] in 2012 who developed a SR-CL system at the BL20 beamline in Spring-8 (Hyogo, Japan). The micro-laminography measurements can be also carried out at other major synchrotron facilities, such as Advanced Photon Source (APS) and Paul Scherrer Institut (PSI).

CL errors associated with dimensional metrology

Like other dimensional measurements, it is crucial to minimise the errors of CL measurements to achieve a high reproducibility. The accuracy of CL measurements depends on potential biased and unbiased errors. Like CT, the uncertainty in CL measurements is also influenced by several factors, including CL system (i.e., stability of source and detector), application operators/engineers, measurement environment (i.e., temperature), and experimental settings (i.e., object geometry) [23]. It should be noted that the errors may also be introduced in post-processing (i.e., the variability of threshold selections).

Image quality comparison between CT and CL

Before implementing the CL scan protocol, images obtained through CL and CT protocols must be compared and verified. Xu et al. [17] examined the image quality acquired by SR-CT and SR-CL at the ESRF nanoimaging beamline (ID22). They conducted a series of experiments and simulations to demonstrate that the orientation of the sample (Ψ) is a critical parameter and CL can produce superior images to CT when there is a limiting angle, Ψ, beyond which the sample is not imaged.

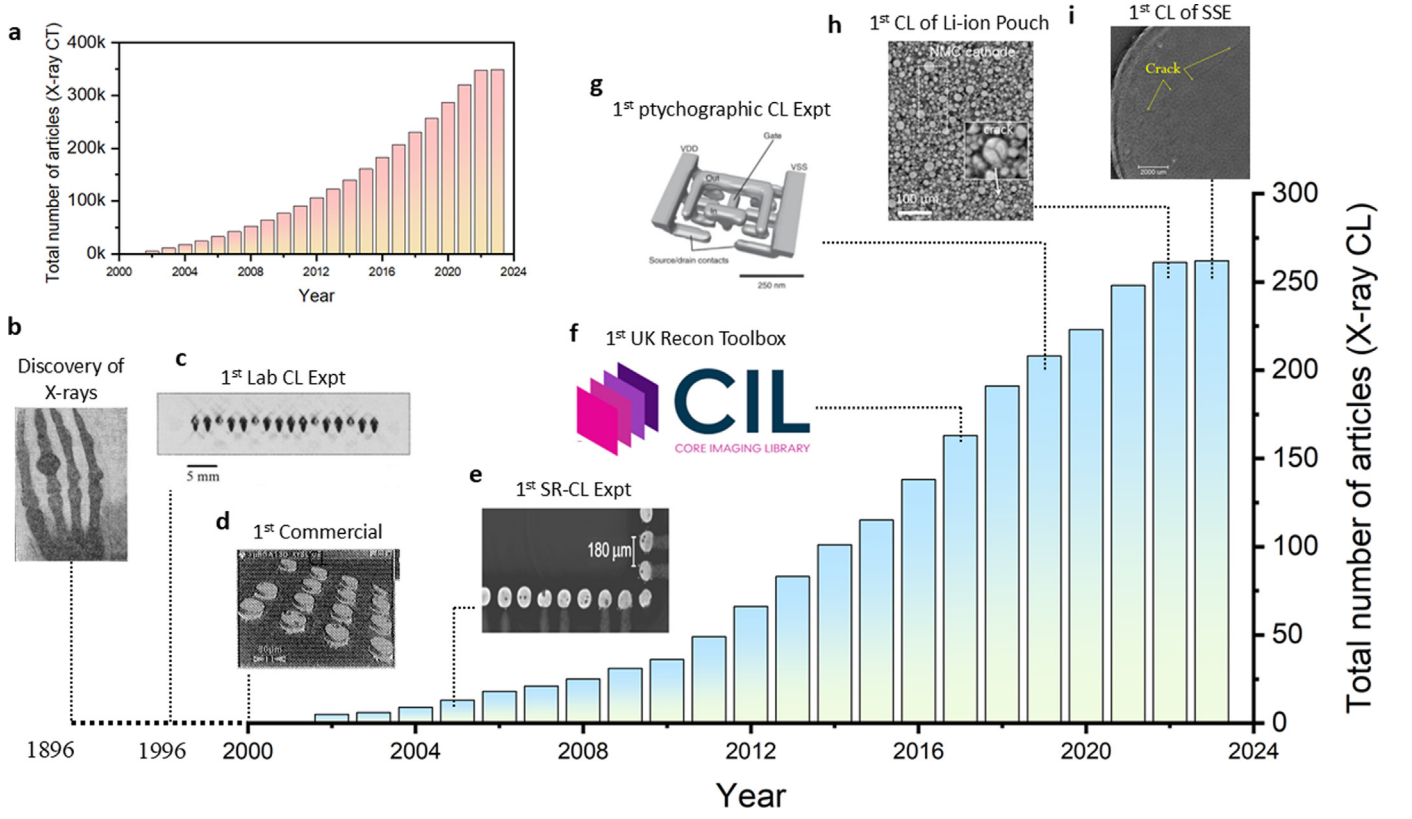

FIG. 1

(a) Notable advancements in X-ray CL, statistics on related CT and CL research publications in the last two decades (Data from Web of Science). The number of CL publications may slightly vary as different terminological names such as fluoroscopy and tomosynthesis were used in the early period. (b) X-ray of a human hand with a ring on the 3rd finger in 1895. (c) Cross-sectional micro-CL slice of solder contacts in a printed circuit board (PCB). (d) X-ray micro-CL application for ball grid array (BGA) inspection using a commercial instrument (desktop system: SkyScan-1080). (e) Synchrotron X-ray micro-CL visualisation of a flip-chip bonded. (f) The launch of the reconstruction toolbox in the UK. (g) The nanostructure of an inverter is rendered in the volume by the high-resolution Ptychographic X-ray CL measurement. (h) High-resolution X-ray micro-CL of the NMC cathode in a battery pouch cell. (h) Micro-CL images of solid-state electrolyte pellet in a pilot-scale pouch cell. Subgraphs have been reproduced with permission from: (b)Wilhelm C. Röntgen [10] with permission from the American Association for the Advancement of Science (AAAS); (f) Zhou et al. [11], (h) Sassov and Luypaert [12] and (e) Helfen et al. [13] with permission from AIP Publishing; (b) Holler et al. [14] with permission from Springer Nature; (c) Zan et al. [15] with permission from the Proceedings of the National Academy of Sciences (PNAS).

Fig. 3 illustrates CL and CT images of a Siemens star resolution test pattern. With identical experimental conditions, CL had a relative consistent contrast when scanning a flat sample. While CT had a non-uniform contrast, this depended entirely on the X-ray direction of the structure. This is also supported by the missing or blurring star pattern (white arrow labelled 1). Also, it was suggested that a small, tilted angle Ψ should be used to minimise artefacts and to balance between the SNR and the artefacts. Smaller Ψ value is preferred so that the objects will yield sufficient SNR.

Overview of CT/CL data processing

Image processing tools

There are numerous tools available for digital image analysis which are summarised in Table 1. In terms of pre-processing, suppliers usually offer exclusive reconstruction software (i.e., Zeiss XMReconstructor and Nikon CT Pro) that can automatically identify centre of rotations (COR) and correct beam hardening (BH) for their own data formats. However, reconstruction can also be carried out using other commercial software, such as Dragonfly. In recent years, customized reconstruction run in a Python environment has been developed to meet different user needs (i.e., CIL). Fiji (ImageJ) [24] is a fundamental post-processing tool and is often used for 2D screening and inspection. Its versatility has been strengthened by a wider imaging community, which enables to perform denoising, contrast adjustment, basic and advanced segmentation (through Weka), object tracing, 3D visualisation, and more. Commercial tools such as Avizo and Dragonfly are expected to provide a superior visualisation experience (compared to open-access software). A number of advanced modules in licensed tools enable researchers to conduct AI-assisted segmentation, image-based simulations, and quantify the reconstructed volumes seamlessly.

Reconstruction

After X-ray CT/CL acquisition, raw projections need to be reconstructed to perform 3D volume rendering. Commercial and/or open-access (OA) software is commonly used for CT data reconstruction (Table 1). However, a commercial software provider usually processes the imaging data collected only by their exclusive imaging facility. For instance, an advanced toolbox (called

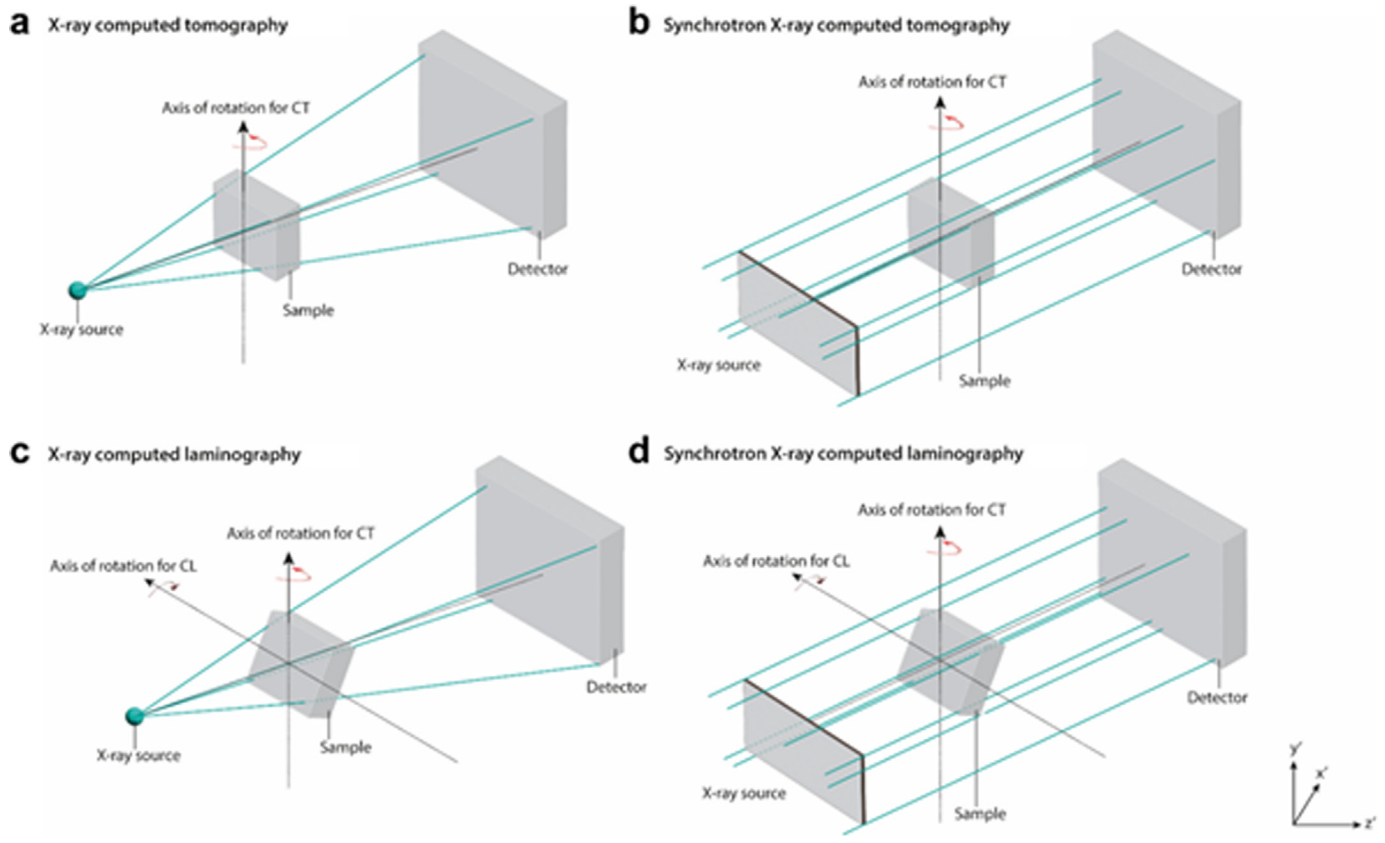

FIG. 2

Schematic diagram of the conventional cone-beam for (a) CT and (c) CL in the laboratory; parallel-beam for (b) SR-CT and (d) SR-CL at synchrotron light source.

TABLE 2

The reported instruments and synchrotron facilities for X-ray laminography.

Instruments/Facilities	Resolution	Application	Reference
Nikon (XT 225)	0.254 mm	Lego blocks	[21]
Sigray (Apex XCT 150)	0.2 μm	Li-ion battery	[15]
ESRF (ID19)	1.4 μm	Flip-chip	[13]
PSI (cSAXS)	14.3 nm	Integrated circuits	[14]
APS (2-BM)	0.92 μm	Mouse brain	[22]
Spring-8 (BL20)	1.5 μm	Copper grids	[20]

'XMReconstructor') was developed by Carl Zeiss to reconstruct data aquisition in the 'txrm' format using the filtered back projection (FBP) algorithm. Advanced reconstructions (including iterative [25] and deep learning [26] algorithms) were available via subscription to OptiRecon and DeepRecon packages in XMReconstructor [5], which have the potential to offer enhanced image quality. In comparison, the Feldkamp Davis Kress (FDK) algorithm was employed by Nikon Metrology to reconstruct the data within the Nikon CT Pro 3D software. Dragonfly can also provide CT reconstruction capability for data collected by a variety of CT instruments, including Zeiss, Nikon, and North Star, etc.

Unlike established CT techniques, commercial software as applied to CL reconstruction is yet to be developed. Recently, Jørgensen et al. [27,28] developed the CCPi Core Imaging Library (CIL, https://github.com/TomographicImaging) to process the X-ray image data, with a particular focus on data reconstruction, including CT/CL, spectral tomography and digital volume correlation (DVC). The OA library was coded in the Python framework and can be implemented directly within the Python integrated development environment (i.e., Jupyter Notebook and Microsoft Visual Studio) as long as the dependent packages are installed. In Fig. 4, a CL imaged LEGO sample was reconstructed in the CIL using the FDK and fast iterative shrinkage thresholding (FISTA) algorithms. Faragó et al [29] developed an OA toolkit (called Tofu) for CT and CL reconstructions. This tool is optimised for stand-alone GPU workstations and can accommodate parallel and cone beam data.

The reconstruction using an iterative algorithm required considerable computational capacity (e.g. couples of hours per tomoscan). Therefore, random-access memory (RAM) and processing times must be considered [30]. The development of high-performance graphics processing units (GPUs) will help to accelerate the procedure via parallelisation and enable the reconstruction of large volumes of data iteratively [31,32]. Commercial software for CL reconstruction is expected to be available in future with faster speed implementation and a user-friendly interface.

CL reconstruction can be performed using the standard FBP or FDK method [33] since both methods have been the most adopted set of options among all CT reconstruction methods.

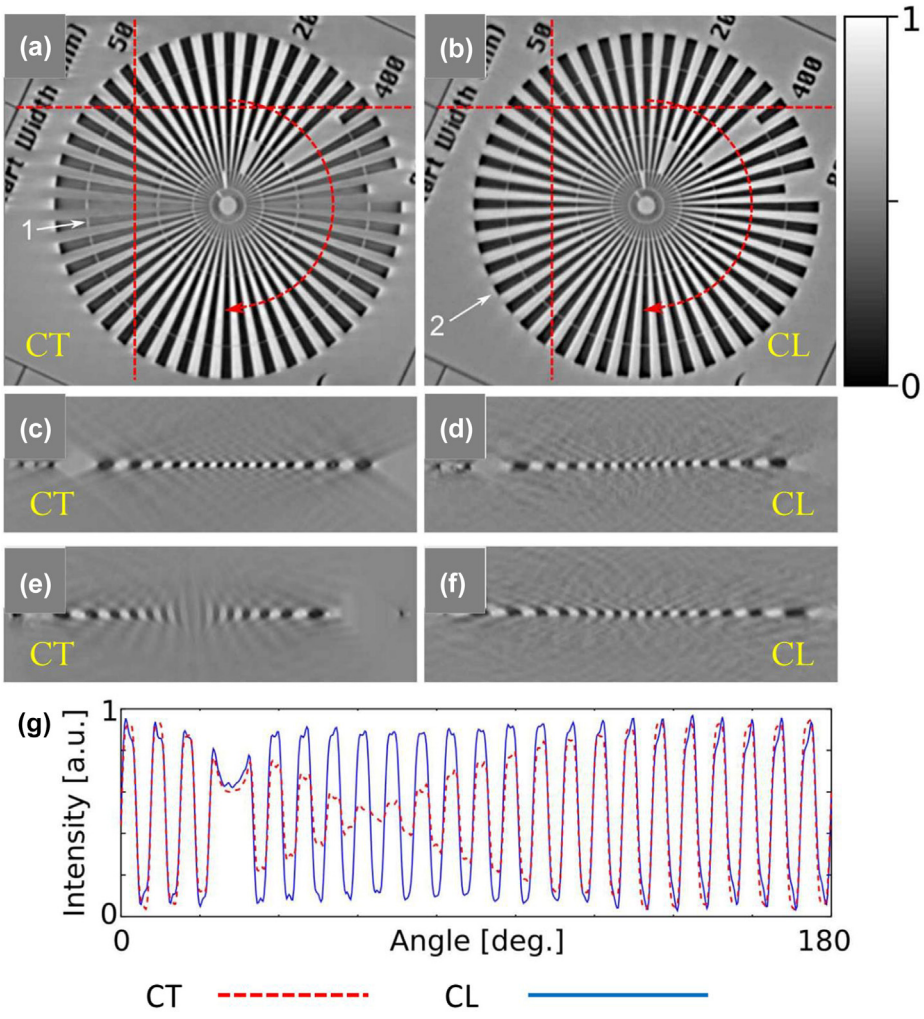

FIG. 3

X-ray CT (a, c, & e) and CL (b, d & f) images of a Siemens star test pattern. The in-plane slices shown for CT (a) and CL (b). Through-plane slices for CT (c & e) and CL (d & f) along the horizontal (c & d) and vertical (e & f) lines shown in (a) and (b). (g) An intensity-angle profile plotted along the semi-circle depicted in (a) and (b) for CT (dashed line) and CL (solid line). The white numbered arrows in (a) and (b) indicate artefacts. This figure has been reproduced from Xu et al. [17] with permission from the OPTICA Publishing Group.

However, the FBP method leads to unsampled frequencies in a double cone region in the reciprocal space. This degrades the spatial resolution in the direction normal to the object plane corresponding to missing frequencies [34]. Unfortunately, the FBP algorithm cannot overcome this issue, thus iterative FBP methods should be preferred. Sun et al. [35] have proposed a conversion method to reconstruct the cone-beam CL data. Their idea is to establish a virtual CT detector that will allow CL data conversion into the projection before the standard FDK method, which can then be applied to the converted datasets.

X-ray CL applications

Metals and alloys

The development of next-generation metallic alloys (such as Mg-, Al- and Ti-based alloys) with high fracture toughness is a crucial to achieve lightweight structures for transportation applications [36,37]. Failure of alloys in service is a direct result of the presence of cavities or voids which evolve under load. Often, voids will accumulate over time when materials are used under continually demanding conditions (i.e., metallic pipes that are exposed to the effects of corrosion and higher pressure below the sea) [38,39]. Visualising these changes can help to determine the locus of the void nucleation sites and the distribution of voids surrounding the grain boundaries.

CT has been widely used to inspect the quality of manufactured components and assembled devices, as well as to conduct reliable dimensional measurements [40,41]. It can determine the dimensions and reveal the internal structure integrity (i.e., material defects) [42]. For instance, *ex-situ* CT has been used to diagnose the defects and/or damage of structural materials [43]. It may also be used to observe *in-situ* the 3D damage accumulation of these metal alloys during processing or loading [2,39,44]. Higher resolution CT techniques can help understand the failure mechanisms, such as cavitation, fracture, and cracking [11,38]. However, an X-ray scan may not be able to penetrate the extended direction of a large planar specimen (which is extended in two directions and thin in the third direction). Moreover, micro-CT may not be compatible in determining genuine engi-

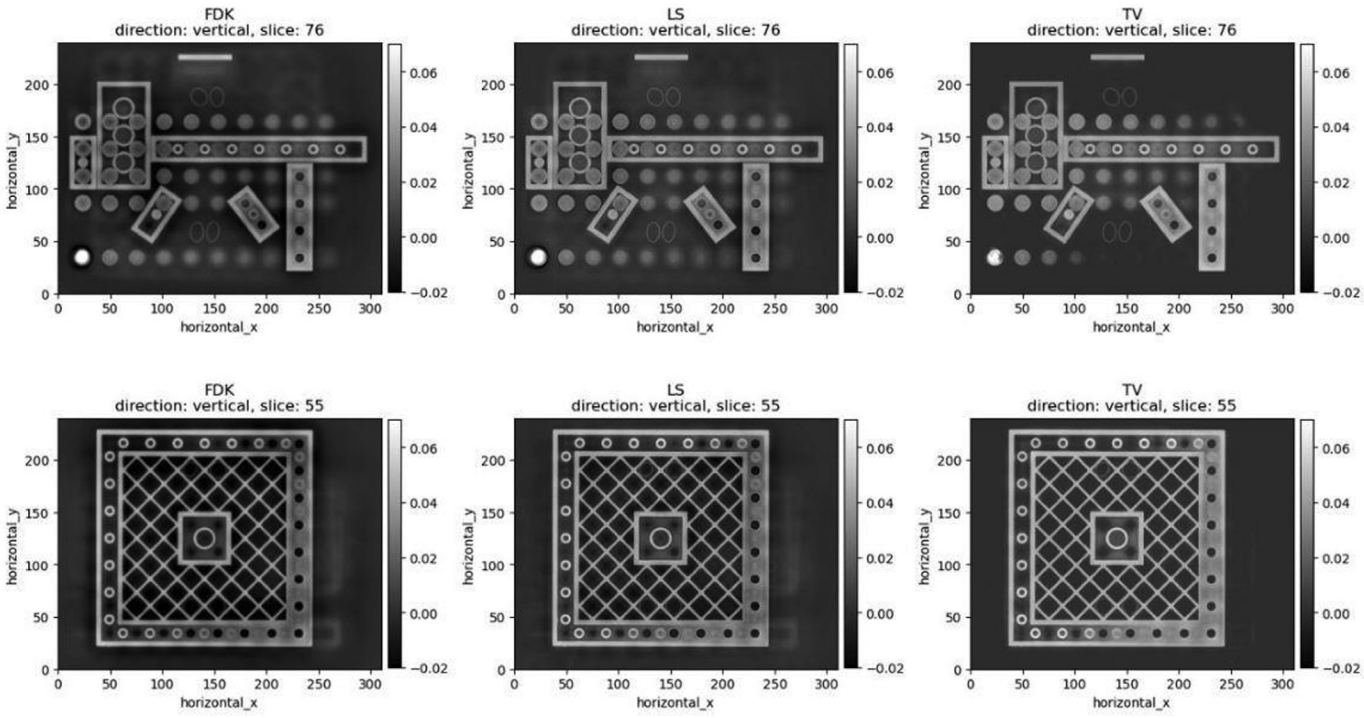

FIG. 4

The graphical user interface (GUI) of CIL in Microsoft Visual Studio. CL reconstruction for a LEGO sample at two different locations (top row and bottom row) using the FDK algorithm, un-regularised Least Squares (LS) and Total Variation regularised Least Squares (TV) with FISTA algorithms. FDK: 1st column, LS: 2nd column, TV: 3rd column. The CL image data was acquired from https://zenodo.org/record/2540509#.Y8h4YeTP2Uk. 2nd and 3rd columns are reproduced from Jørgensen et al. [27], with permission from The Royal Society.

neering failure situations where plastic zone sizes may reach the order of several millimetres in both metal and other materials [45].

Applying the X-ray CL technique can address sort of the issues [46–48]. For instance, Ueda et al. [45] followed and visualised void evolution in an Al-Cu-Mg alloy (for aerospace applications) at the initiation of a crack and its propagation using micro-SR-CL at ESRF. A tilted angle (ca. 25°) of the sample rotation axis was used to obtain a voxel size of 0.7 μm for a large sample (millimetres in size). Fig. 5 shows the 3D microstructural evolution of an individual void at the centre of the flat sample against its loading steps. They proposed that the formation and coalescence of voids led to a shape change that negatively affected the material life. SR-CL enabled the quantification of microscopic void behaviours at various positions with load histories in a large flat sample to understand the metal failure mechanisms. Moreover, CL images can be used to provide 3D geometry for achieving reliable computational models [49].

Polymer composite and other applications

To achieve a longer cruise mileage and reduce associated fuel consumption and cost for aerospace applications, polymer composites have increasingly been used to replace light metals (i.e. Ti and Al alloys) [50]. According to Mangalgiri et al. [51], nearly one-third of the structural weight of some aircrafts can compromise fibre-reinforced polymer composites. The composites must withstand long-term service in harsh aerospace conditions (i.e. extreme temperature conditions from −30 to 370 °C) [37].

The incorporation of a fibrous secondary phase into the polymer matrix is a mature approach to increase material toughness. Nevertheless, polymer composites suffer impact damage that ultimately leads to internal macroscale failure, such as delamination [52]. Understanding internal interfacial failures and the effectiveness of toughening mechanisms in more detail is important in the development of next-generation composites with substantially improved performance.

In these circumstances, *in-situ*, high-resolution micro-CT technologies could be used to directly examine the incremental damage inside the composite samples during life [53–55]. However, there is always a compromise in the sample geometry for it to be suitable according to the CT scanning protocol. Considering the previous metallic alloy case, it is far more pragmatic to inspect a planar specimen (typical of aerospace components) using the CL and SR-CL techniques [56–58].

A realistic scenario of composite fracture can be reproduced and captured using the CL technology. This was achieved by Borstnar et al. [59] who studied the fracture evolution of carbon fibre reinforced polymers (CFRP) using both phase-contrast SR-CT and SR-CL tools at the TOMCAT beamline in the Swiss Light Source (Villigen, Paul Scherrer Institute) and at the ID19 beamline at ESRF, respectively. They used identical beam energies (i.e., 19 keV monochromatic beam) except for the CL implementation where a tilted rotation was used. In Fig. 6, the high resolution of SR-CL with a large FOV enables the identification of the fracture in these CFRP materials. The failure of CFRP demonstrates that interlaminar fracture is the result of a zone of activity

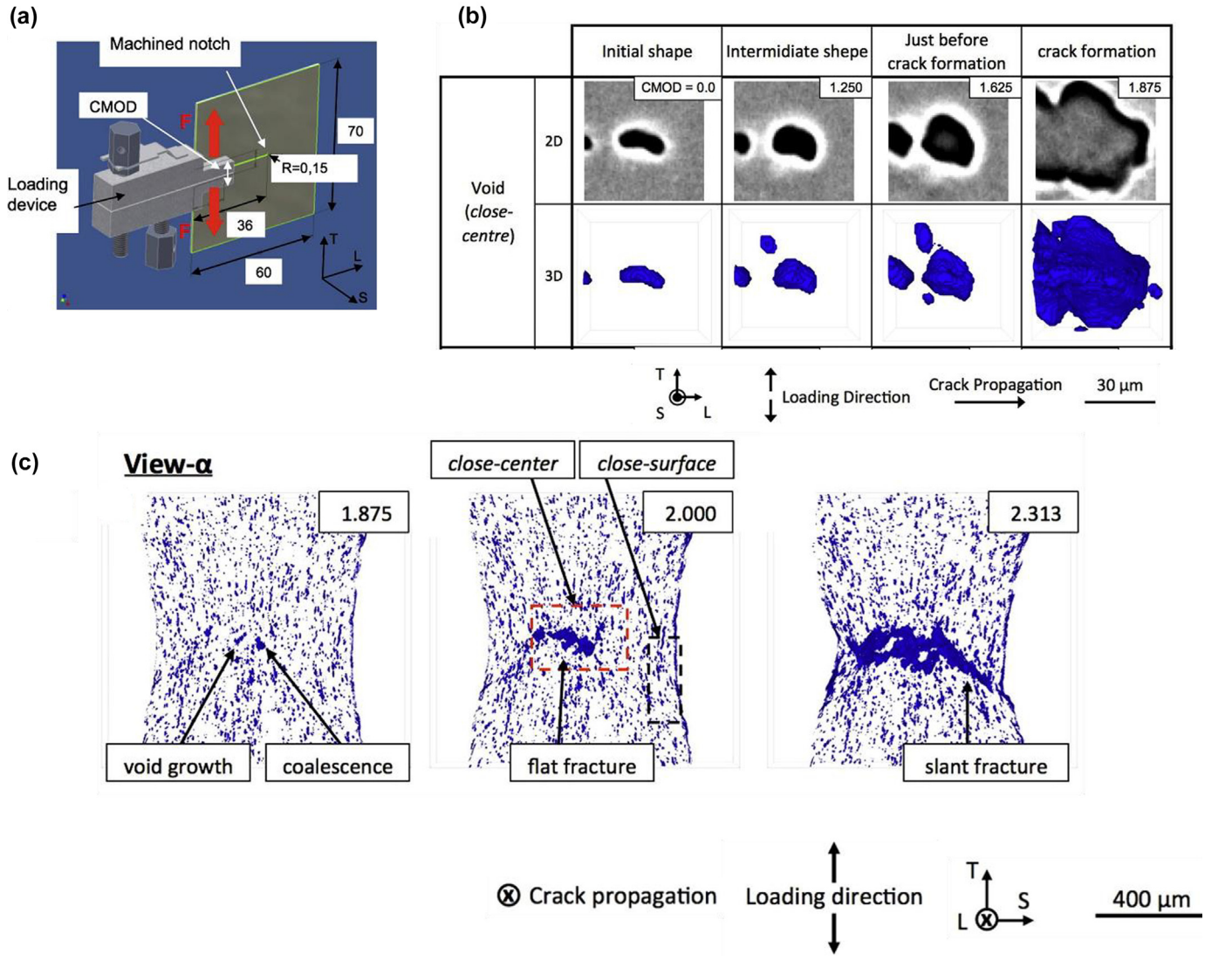

FIG. 5

(a) Schematic diagram of *in-situ* loading setup for SR-CL, with the dimension of 60 x 70 x 1 mm^3. (b) 2D sectional slices and 3D images with 28 μm thick of the extracted voids in the middle regions for different loading steps in the selected region of interest (ROI). All slices are extracted in the middle of the 3D tomogram, and 3D voids are rendered in blue. (c) 3D crack propagation and void evolution (rendered in blue) in the sheet metal. This figure has been reproduced from Ueda et al. [45] with permission from Elsevier.

rather than a single crack tip. Interestingly, they compared the failure mechanisms at the microscale between two sample geometries using the SR-CT and SR-CL tools [59,60]. One sample with a cross-section of 3 × 1 mm was used for SR-CT, whereas a wider cross-section (3 × 20 mm) sample was used for SR-CL. This extended lateral area enabled capture of the actual fracture from micrometre to the millimetre length-scales, which lies in close proximity to practical applications.

Nevertheless, the unique dimensional ability of X-ray CL to image flat objects can be used to validate the CT observations (a narrow cross-section for CT sample) as well as reveal comprehensive behaviours that CT cannot fully characterise. Fracture behaviour obtained via CT may not be completely representative. Furthermore, a dual-energy beam could be used to characterise the matrix phase and reinforced phase, which provides further sensitivity information to understand the failure mechanism of advanced composites.

SR-CL finds another interesting application in botany. A study was conducted by Verboven et al. [61] in 2015, where they used SR-CL to illuminate the structure of tomato leaves (specifically two different genotypes) at ID19 in the ESRF. Given that there is strong absorption of X-rays in the lateral directions, this proves problematic for the study of leaves with longer extensions. However, with the aid of the SR-CL technique, the tilted rotation mechanism allowed their team to achieve a pixel resolution of 0.75 μm and a large FOV of up to 1 mm^2. Due to (1) the high resolution of SR-CL and (2) the phase-contrast imaging mode (materials with small differences in attenuation coefficient could be resolved), it was possible to differentiate spongy and palisade mesophyll cells and describe their interconnectivity. As the synchrotron source incorporates a monochromatic beam there was also a substantial reduction in imaging artefacts and a much higher resolution achieved.

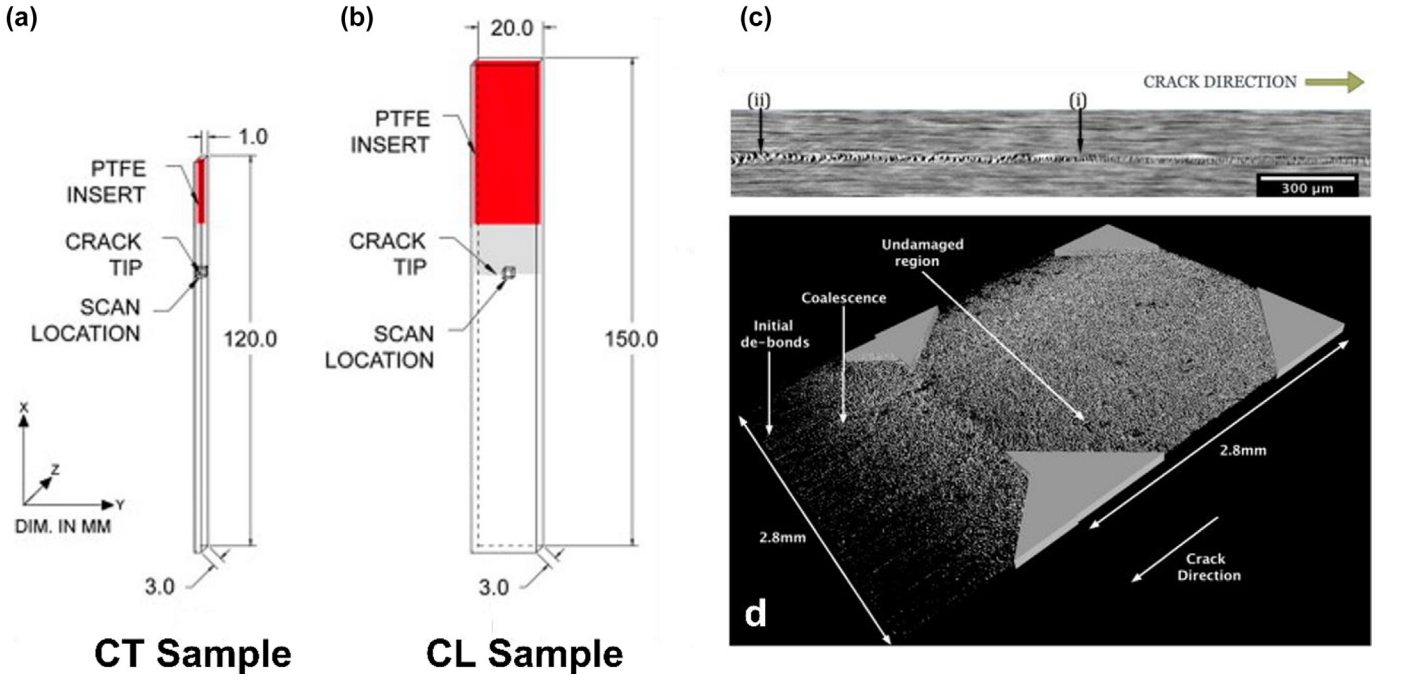

FIG. 6

Two specimens with different geometries were used (a) for SR-CT (120 × 3 × 1 mm^3) and (b) for SR-CL (150 × 20 × 3 mm^3) measurements. The CL sample is laterally extended, which is closer to the practical component and structural length scale. Images obtained by SR-CL show (c) the discontinuous behaviour behind the crack tip in 2D and (d) the cracks and distribution in the process zone in 3D. This figure has been reproduced from Borstnar et al. [59] with permission from Elsevier.

In Fig. 7, the SR-CL images reveal the mesophyll connectivity and pore space network in 3D. From Fig. 7(c) and (d), this work demonstrates that image-based simulation could be applied to the data obtained by CL technology. They proposed that the 3D models of leaf anatomy from intact leaves can be used to explain the effect of leaf anatomy on plant hydraulics, gas and metabolite transport as well as provide further details of the functional value of different anatomical features. For example, from the 3D microstructural studies it was found that chloroplast movement depends on the level of light intensity and this in turn affects the CO_2 distribution within the plant cell [62]. Another similar study in the field of botany and specifically leaf anatomy was reported by Harasse et al. [63] in 2012. Here, the SR-CL was also employed but achieved a lower resolution of 4.34 μm.

Electrochemical devices

Electrochemical energy storage devices, such as battery [64] and fuel cell [65] technologies, will play a decisive role in achieving electrification and decarbonisation in the next decade, with applications ranging from power stations, electric vehicles (EV) to portable electronic devices. Currently, internal combustion engine (ICE) vehicles are being replaced by an increasing number of EVs. Hence, it is pivotal to understand the failure mechanisms and the microstructure evolution of Li-ion battery technologies before developing next-generation EV batteries with lower cost, higher safety, and longer driving range per full charge [66].

Many different types of batteries and cells (i.e., coin cell, pouch cell, prismatic cell, and cylindrical cell) are used in both research and industrial settings. Given the limitation in EV space and weight, the pouch type Li-ion battery accommodates electrode materials with minimal space lost and is considered one of the best candidates for EV applications. For instance, BYD Auto Co., Ltd developed the blade battery that can optimise their cell-to-pack (CTP) technique. Diagnostic tools such as acoustic [67] and laser imaging [68] are proven to be the most feasible in detecting gas generation and electrolyte wetting in the pouch with a power of up to tens of amp hours (Ah). X-ray imaging can also provide comprehensive information across multiple lengths and time scales to interrogate cell degradation [69,70]. However, the importance of carrying out microstructural observations in 3D is clear and has been demonstrated in Li ion batteries many times previously [71]. For instance, particle crack initiation [72,73], the interconnected porous morphology of the electrode [74,75] and their structural evolution or degradation [76,77] all benefit from 3D microstructural analysis, which often require some opening of the battery for preparation of more optimal samples for X-ray CT [78].

However, non-destructive CT investigations of the interior structure of battery pouch cells over their life cycle is still challenging, especially for much larger pouch formats [79] (i.e., Nissan LEAF cell with a size of 261 mm × 216 mm × 8 mm). Again, this is mainly due to geometric limitations; when one scans a high-aspect-ratio pouch, the image contrast will be severely deteriorated due to the higher absorption of the X-ray along and through the extended direction. Also, the combination of low-density (i.e., graphite and silicon) and high-density materials (i.e., $LiNi_{0.8}Mn_{0.1}Co_{0.1}O_2$ (NMC811)) pose a challenge in obtaining differential image contrast. Recently, Zan et al. [15] demonstrated this pioneering application of high-

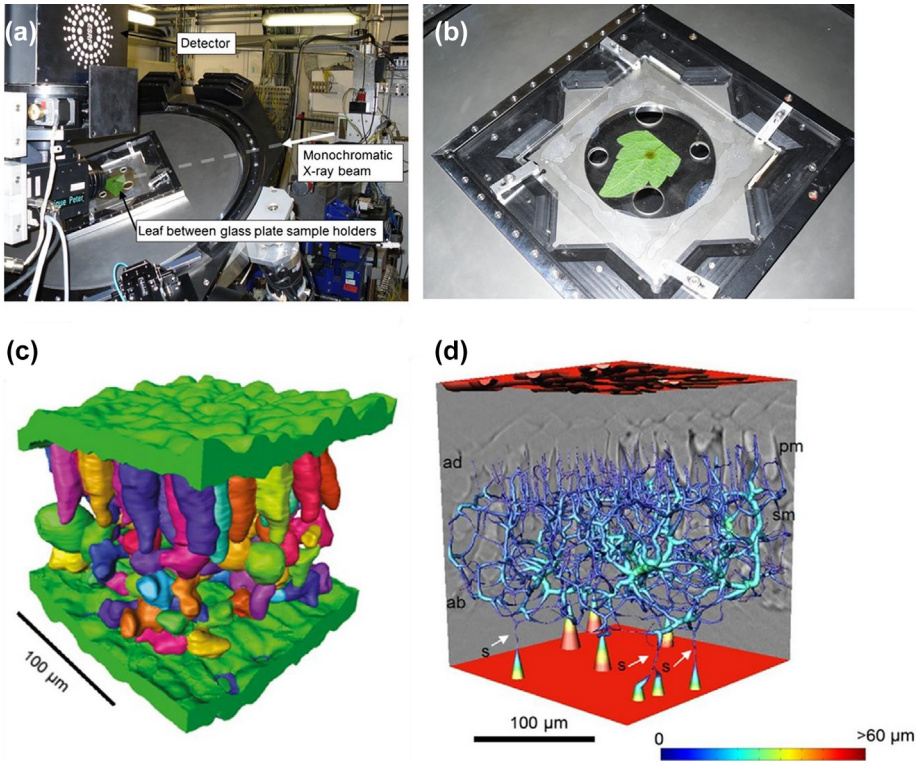

FIG. 7

(a) The experimental setup for SR-CL imaging the leaf specimen. (b) The zoomed-in graph shows the sample holder with a leaf. (c) The 3D cellular structure of the mesophyll with a voxel size of 0.75 µm. The epidermis is assigned in green, whilst individual cells are coloured randomly. (d) Image-based modelling shows the pore network of a tomato leaf in 3D. The colour scale of the network indicates the local radius of the pore channel inside the leaf tissue. This figure has been reproduced from Verboven et al. [61] with permission from Wiley.

resolution lab-based micro-CL to observe the interior structure of the electrodes in a miniature Li-ion pouch cell (50 mm width). In Fig. 8, they captured the microstructure of both NMC cathodes and anodes at a spatial resolution of 0.5 µm. This suggests that the CL technique is sufficient in resolving fine-scale particulate cracks and voids in individual electrode particles. Usually, to achieve sub-micro information, the cell has to be dismantled to extract the electrode materials for a CT scan. However, CL can be used to avoid the destructive process and generate comparable results obtained by micro-CT without opening the Li-ion cell.

CL Exploitation

In late 2020, the authors initiated their CL journey by forging a collaboration with the UK Henry Royce Institute for Materials. Researchers began to develop X-ray CL related packages for energy storage devices, from CL image acquisition to the data reconstruction phase. Here, the CL work is being performed on a high-energy lab X-ray instrument (Nikon XT 225) which can accommodate larger objects with dimensions of up to tens of centimetres. This work is being carried out in collaboration with researchers from and the University of Oxford (Department of Materials) and the Science and Technology Facilities Council (STFC). The main objectives are: (1) to develop and understand X-ray CL capability in the laboratory, (2) to verify the viability of lab-based CL for battery pouch cells and perform CL scans to obtain morphologies and structures. As the Nikon scanner does not have inherent CL protocol capabilities, two options exist to implement the CL scan and tilt the stage. A custom-built inter process communication (IPC) interface, developed by Gajjar et al. [80], could be used to tilt the stage. Under this protocol, a GUI of IPC replaces the VB based programming that can manipulate the Nikon scanner. Another approach is to modify the system setting to tilt the stage from 0 to 30° with due caution.

Previous studies have demonstrated CT is a powerful tool to detect the crack formation and growth using some bespoke cells [81]. For example, a sample of a solid electrolyte for a solid-state battery (Li/ Li_3PS_4/Li) was assembled using a 1/8 Swagelok cell for *operando* 4D SR-CT [82]. Although 3D evolution of microscale cracks was successfully followed, direct observation of crack propagation at lateral direction was restricted after reaching the geometric limitation of the sample (diameter of 2.5 mm). Here, CL has potential to resolve the above challenge to understand the materials failure in real-life application without compromise the cell design (Fig. 9). To realise our idea of using CL to track the cracks in a high-aspect-ratio sample, a prototyping pouch type of solid-state battery was fabricated for CL imaging. Laboratory CL images of two large-size solid-state pouch batteries (150 mm × 90 mm × 0.2 mm) are taken for demonstration and comparison. The cell was assembled in an argon filled glove-box and sealed into a pouch under vacuum, including a LPSCl ceramic pellet (Li_6PS_5Cl, sulfur-based solid-state electrolyte). The LPSCl pellet was fabricated by applying the field-assisted sintering technique (FAST). The CL scan (Fig. 9a) was carried out

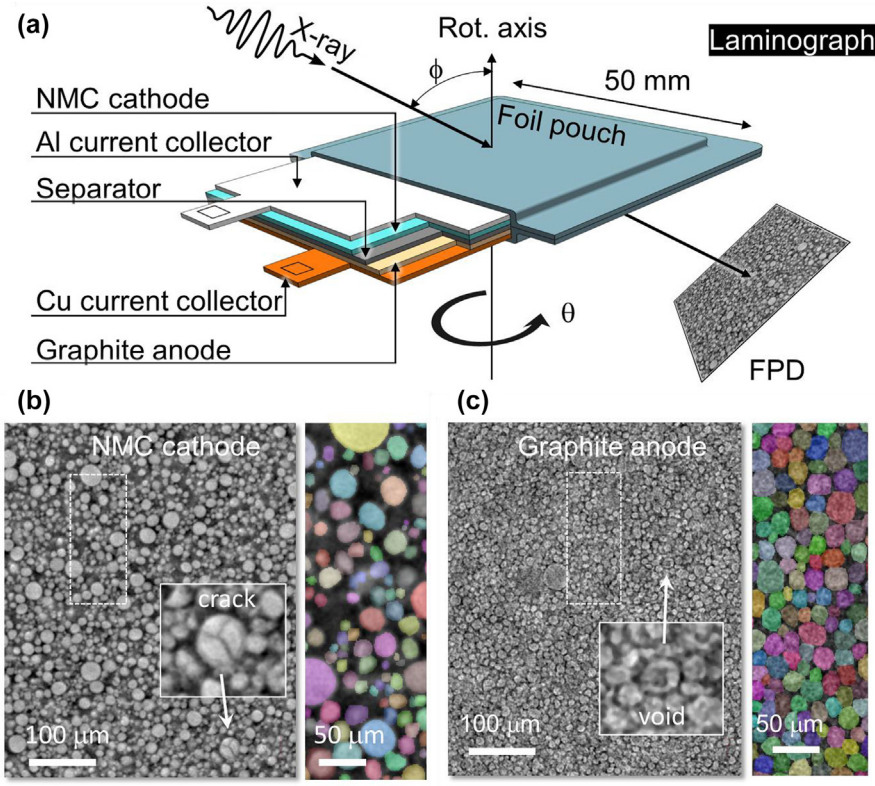

FIG. 8

(a) The experimental setup for CL imaging a Li-ion pouch cell. The 2D microstructure of (b) NMC cathode and (c) graphite anode, with the image segmentation of active particles. This figure has been reproduced from Zan et al. [15] with permission from the Proceedings of the National Academy of Sciences (PNAS).

using a tungsten target, a voltage of 100 kV, resulting in a total power of 9 W. In total, 600 projections were obtained with an exposure time of 1 s per projection. The pellet was maintained within the FOV to obtain a spatial resolution of ca. 16 μm. The FDK method was used to reconstruct our LPSCl sample. For future *operando*/*in-situ* CL experiments, a bespoke holder has been made by a 3D printer to accommodate the flat pouch for cycle-induced strain–stress analysis.

Whether using the lab or synchrotron sources, the application of CL is opening up an opportunity to understand the microstructure and to correlate 3D data with the electrochemical performance. As demonstrated in Sections 4.3, CL can provide a unique approach to imaging the entire electrode sheet up to a few centimetres without the need for trimming and machining. In other words, CL can directly obtain the microstructure from a pouch cell with identical spatial resolution, whereas CT is almost incapable of imaging a pouch cell, and *ex-situ* samples have to be prepared by a micro-laser or FIB [83]. CL imaging technique naturally avoids such processes and thus reduces the uncertainty during the sample preparation. Moreover, CL ensures that the battery microstructure information can be procured down to the submicron scale, with the adjusted distance between the X-ray source to sample and the installation of additional lenses for achieving two-stage magnification. We envisage that CL will play a key role in supporting the development of next-generation all-solid-sate batteries.

Conclusion, challenges, and outlook

Concluding marks

We provide a brief review of the CL technique, covering its history, principles, data analysis, software and toolkits, and potential applications. X-ray CL has made significant advancements over the last two decades, with spatial resolution drastically improving to resolve a micro-feature in a large flat sample. Thanks to 4th gen synchrotron sources that provide high brilliance and flux, dynamic probing and observations are now enabled benefiting from improved temporal resolution. Despite the hardware progress, the availability of open source and proprietary software toolboxes for CL reconstruction remains limited, which restricts the practical applications. This is expected to improve with the development of user-friendly GUIs provided by instrument manufacturers. Currently, rudimentary metrics can be extracted to quantify the geometrical and temporal features of their CL images. It is anticipated that AI will be integrated into existing pipeline in near future, which offers a pathway to improve the effectiveness and throughput of the CL technique. Furthermore, CL image-based modelling and finite element (FE) simulations are expected to be used for generating a deeper understanding of structural change. These approaches have been widely deployed for CT [84]. Nevertheless, there is no doubt that the development and application of X-ray CL is likely to grow rapidly (following a trajectory similar to its CT counterpart). The growth will be particularly notable for tracking structural evolution over time in materials and devices

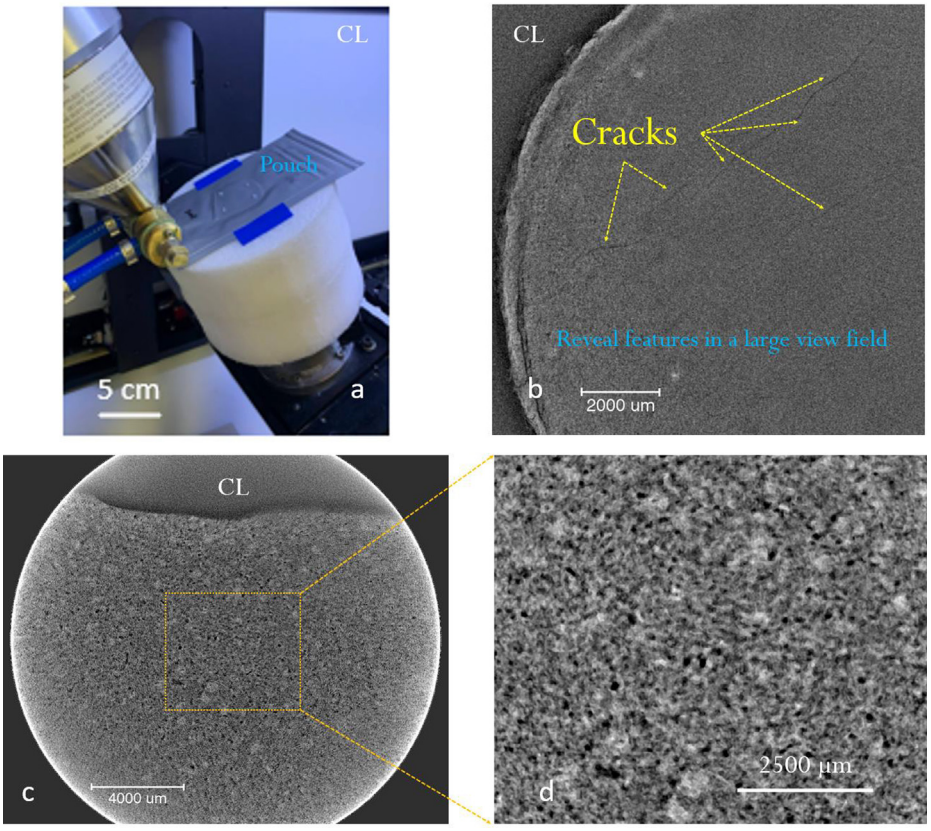

FIG. 9

Laboratory X-ray CL imaging of a prototyping solid-state pouch cell (a) The experimental setup (b) The microstructure of LPSCl pellet. The Li_6PS_5Cl (sulfur-based SSE) was sealed in a pouch with a size of 150 mm × 90 mm × 0.2 mm. The as-manufactured cracks were resolved. (c) A higher resolution of CL to reveal the morphologies of another LPSCl pellet. (d) Zoomed-in section of (c) shows the porosity and voids within the pellet.

with high-aspect-ratio. The CL technique will play an indispensable role in battery development.

Multiscale, multi-modalities, correlative imaging techniques in batteries

To resolve outstanding challenges in materials science and device development and optimisation, it is necessary to study morphological evolution at a range of length scales over time and recording different types of information [69,85–87]. For example, for battery research, information is needed from the particle level to the electrode and finally to the cell level. Correspondingly, multi-scale correlative imaging techniques are a practical solution to bridge such challenges in scale [88–91]. Multiple ROIs can be acquired in an intact device to determine the local heterogeneity, which has been previously demonstrated using modern systems combining 3D microscopy technique (with RaaD capability) and nano-imaging [5,92].

It has become well recognised that the application of non-destructive industrial (macro) CT, micro-CT, and nano-CT can be applied usefully to visualise and quantify the battery cell deformation and delamination [77,93], the tortuosity of the electrode that governs the ion transportation [74], and individual particle cracks [94]. Appreciating these parameters can help understanding of as manufactured quality as well as battery failure mechanisms in service. Currently, X-ray CT has a resolution limitation (>50 nm, Zeiss Ultra 810) and is unable to resolve materials with similar X-ray attenuations. As an alternative tool, nanoscale lens-less X-ray imaging (down to 10 nm [95]) can compensate for insufficient CT resolution, which was previously demonstrated in 2020 by Muller et al. [96]. They observed a thin layer called solid electrolyte interface (SEI) growth on a silicon particle after cycling via ptychographic X-ray CT (PXCT). In 2019, Holler et al. [14] applied ptychographic X-ray CL (PXCL) to achieve even higher resolution for a representative sample size. In 2020, Witte et al. [97] employed the soft X-ray CL (E < 1 keV) to image nanoscale thin specimens. Future endeavours will focus on realising *in-situ* or *operando* PXCT/CL studies.

In principle, battery materials, such as Li-sulfur and solid-state electrolytes, are extremely sensitive to ambient environments. Results will only remain robust if the electrode materials can be sealed in an air-insulated sample holder before characterisation. In compassion to CL, high-aspect-ratio tomography (HART) [5] could be an alternative option to obtain metrology information (i.e., electrode assembly and alignment) in a commercial battery pouch. Although tomography is a non-destructive tool, the design and geometries of the cells often have to be compromised (sometimes may involve a destructive process) to obtain high-quality, high-resolution CT images [98]. In particular, a typical nano-CT demands a high standard of sample preparation at the expense of the FOV [83], which requires dismantling a large sample down to the tens of micrometres. In contrast to CT, CL has less restriction in sample preparation and scanning of an

intact electrode sheet with a larger FOV can occur, thus making the result more representative. X-ray CL can also be used for high-throughput inspection since fewer X-ray projections will be needed (and they will be much faster compared to CT). Hence, we believe that multi-scale CL imaging can be implemented either in the laboratory or at synchrotron sources. This will pave a new route to capturing ageing details in a large-format pouch cell.

The development of multiple imaging modalities could advance battery research and many related fields. Neutron computed laminography (NCL) was applied to materials research in 2011 [99] due to the high neutron sensitivity to low atomic number materials such as H and Li [100,101]. NCL can be used to perform energy-selective measurements [102], which will be useful for understanding the lithium intercalation upon state of charge (SOC) in Li-ion pouch batteries. A focused ion beam SEM (FIB-SEM) is a destructive sectioning method but with a higher spatial resolution than X-ray CT or CL [103]. It can be combined with energy-dispersive X-ray spectroscopy (EDS) and electron backscatter diffraction (ESBD) techniques to obtain chemical compositions and grain orientation [104]. The recent development of the hierarchical CT/CL technique at ESRF allows for the characterisation of a large object across multiple lengths with a resolution down to the micron level [105–107], which will open up an excellent opportunity, for example to image a full-size pouch cell.

The development of dual-energy X-ray CL/CT, where two tomograms can be collected either in sequence or simultaneously at two accelerating voltages [108] will further enhance the imaging capabilities for these applications. It is envisaged that this will be useful for CL imaging of an electrode material that contains both high and low attenuating phases (i.e., Ni, Co and Mn, along with carbon and polymer binder in the cathodes, and Si and graphite in the anodes). There is an emerging opportunity to develop spectral CL and hyperspectral CL techniques [109,110], which will provide valuable information in terms of elemental and chemical composition.

Dimensional X-ray CL

There are a plethora of studies following the evolution of 3D structures over time (termed 4D X-ray CT) [76,111,112], such as the dissolution and re-deposition of sulfur particles in the Li-sulfur cell [113]. X-ray imaging can either be undertaken in a time-lapse manner (termed *in-situ* 4D X-ray CT) or continuously in a real-time manner (termed *operando* 4D X-ray CT). However, the *operando* measurements can only be performed at synchrotron sources due to the high temporal resolution required. Examples include investigation of the catastrophic thermal runaway failure of a battery [114,115]. As described in Section 2, it is believed that the conception of 4D X-ray CT can be directly transferred and applied to X-ray CL, which will be termed 4D X-ray CL [116,117]. Authors have collaborated with researchers from ESRF-KIT to perform 4D *in-situ* experiments on all-solid-state pouches (proposal No. MI-1502). With the high-fluxes and fast readout detectors available at 4th generation synchrotron facilities, it is even possible to image chemical and structural changes occurring in cells during their operation in real-time [118,119]. It is anticipated that bespoke environments designed by users will be integrated into lab and synchrotron CL techniques to maximise the advantages.

Artificial intelligence in the CL application

Artificial intelligence (AI) has been widely used in computer vision and digital image analysis as numerous studies integrate the AI technique and multiscale imaging characterisations for energy materials [91,120–122]. Unfortunately, the application of AI in CL has not yet been published in the open literature, which implies that there is a significant opportunity to apply AI techniques to advance CL characterisation, as the advantages offered by DeepRecon and DeepScout algorithms have been previously demonstrated as an illustrative example.

AI-empowered techniques, such as machine learning (ML) and deep learning (DL), can learn from input images and generate models (termed 'data-driven models') after training. AI has demonstrated its powerful capability and versatility in accelerating the understanding of materials microstructure and having the following applications: (1) DL-based reconstruction has been used to minimise image artefacts and noise [26,123]. (2) Acquiring high-quality images is challenging due to instrumental limitations. A trade-off between the spatial resolution and representative volume (or the FOV) prevents extraction and validation of metrics. However, the AI technique may provide a solution to address the length scale issue and could generate super-resolution CT images [124]. One can take a high-resolution CT/CL image and employ AI to decipher structures and morphologies to generate a model. Then, the pre-trained model can be applied to the low-resolution CT/CL images to re-create an artificial image with higher quality. For instance, generative adversarial networks (GAN) [125] have gained a growing interest due to their ability to increase dataset size by regenerating new high-quality images from the initial image sets, which can be used as data augmentation of a training dataset. This will significantly reduce the acquisition time and lower the cost, overcoming the blur of low-quality images while maintaining a large representative volume. (3) Compared to manual image segmentation, AI-based segmentation of CT/CL images can provide more robust structural information and statistical confidence [126]. For instance, using AI-based algorithms to separate and classify the multiple phases with similar X-ray attenuation [127–129]. Also, ML/DL techniques provide sensitivity in segmenting the 3D CT/CL images with complex morphologies [130]. It is common to train a 2D/3D model using the random forest (RF) and convolutional neural networks (CNN) architectures [131]. It is anticipated that the AI-assisted approach will be included in the workflow of X-ray CT/CL imaging. Currently, the main challenges and limitations in AI-based studies are insufficient ground truth data to train and augment the model, the contradiction between the requirement of model generalisation ability and the different data sets. It should be considered the ethical uses of generative AI tools and implications, such as data transparency, fairness, and accountability.

Author contributions

WD and **PRS** conceived the idea. **WD** and **MM** conducted the literature review and wrote up the original manuscript. **WD** and

FI performed the measurement and reconstruction. **BF** prepared the pouch sample. **MM**, **JB**, **SF**, **SZ**, **GF**, **EP** discussed and revised the original manuscript. **PSG**, **RJ**, **DJLB**, and **PRS** secured the grants, reviewed, and edited the manuscript.

CRediT authorship contribution statement

Wenjia Du: Writing – original draft, Visualization, Validation, Software, Project administration, Methodology, Investigation, Formal analysis, Data curation, Conceptualization. **Francesco Iacoviello:** Investigation, Formal analysis. **Mateen Mirza:** Writing – original draft. **Shangwei Zhou:** Investigation, Data curation. **Junfu Bu:** Methodology, Investigation. **Shikang Feng:** Investigation. **Patrick S. Grant:** Writing – review & editing, Resources, Funding acquisition. **Rhodri Jervis:** Writing – review & editing, Funding acquisition. **Dan J.L. Brett:** Writing – review & editing, Funding acquisition. **Paul R. Shearing:** Writing – review & editing, Supervision, Funding acquisition, Conceptualization.

Data availability

Data will be made available on request.

Declaration of competing interest

The authors declare that they have no known competing financial interests or personal relationships that could have appeared to influence the work reported in this paper.

Acknowledgements

The authors would like to acknowledge the EPSRC grants for supporting the emerging energy works at the Electrochemical Innovation Lab (EP/R020973/1, EP/S018204/1). The Faraday Institution grants (EP/S003053/1, FIRG027, FIRG057, ReLiB project website: https://relib.ac.uk/ & https://www.faraday.ac.uk/research/lithium-ion/recycle-reuse/). The initial discussion and help from Dr Parmesh Gajjar and Professor Philip Withers are much appreciated. We also thank the discussion and technical support from the CCPi team (Dr Edoardo Pasca, Dr Gemma Fardell, and Dr Jakob S. Jørgensen). WD thanks the PDRA Enrichment Award from the Alan Turing Institute. SZ acknowledges the Chinese Scholarship Council (202108060113) for funding support of his PhD. PRS and DJLB acknowledge the Royal Academy of Engineering funding for supporting their respective Research Chairs (CiET1718/59 and RCSRF2021/13/53).

References

[1] P.J. Withers et al., Nat. Rev. Methods Primers 1 (1) (2021) 1–21.
[2] E. Maire, P.J. Withers, Int. Mater. Rev. 59 (1) (2014) 1–43.
[3] S. Stock, Int. Mater. Rev. 44 (4) (1999) 141–164.
[4] H. Villarraga-Gómez, E.L. Herazo, S.T. Smith, Precis. Eng. 60 (2019) 544–569.
[5] H. Villarraga-Gómez et al., J. Fail. Anal. Prev. 24 (5) (2024) 2113–2128.
[6] J.T. Dobbins III, D.J. Godfrey, Phys. Med. Biol. 48 (19) (2003) R65.
[7] B.Z. Des Plantes, Acta Radiol. 2 (1932) 182–192.
[8] J.T. Dobbins III, Med. Phys. 36 (6Part1) (2009) 1956–1967.
[9] S. Gondrom et al., Nucl. Eng. Des. 190 (1–2) (1999) 141–147.
[10] W.C. Röntgen, Science 3 (59) (1896) 227–231.
[11] J. Zhou et al., Appl. Phys. Lett. 68 (24) (1996) 3500–3502.
[12] A. Sassov, F. Luypaert. X-ray digital microlaminography for BGA and flip-chip inspection, in: AIP Conference Proceedings. American Institute of Physics, 2000.
[13] L. Helfen et al., Appl. Phys. Lett. 86 (7) (2005) .
[14] M. Holler et al., Nat. Electron. 2 (10) (2019) 464–470.
[15] G. Zan et al., Proc. Natl. Acad. Sci. 119 (29) (2022) e2203199119.
[16] L. Yenumula, U. Kumar, A. Dash, X-ray industrial computed laminography (ICL) simulation study of planar objects: Optimization of laminographic angle, in: Industrial Tomography and Instrumentation Section, Isotope Production and Applications Division, Bhabha Atomic Research Centre, 2015.
[17] F. Xu et al., Opt. Express 20 (2) (2012) 794–806.
[18] T. Wang et al., IEEE Trans. Nucl. Sci. 64 (10) (2017) 2742–2760.
[19] N.S. O'Brien et al., J. Xray Sci. Technol. 24 (5) (2016) 691–707.
[20] M. Hoshino, et al. Development of an X-ray Micro-Laminography System at SPring-8, in: AIP Conference Proceedings, American Institute of Physics, 2011.
[21] S.L. Fisher et al., Meas. Sci. Technol. 30 (3) (2019) 035401.
[22] V. Nikitin et al., J. Synchrotron Radiat. (2024) .
[23] P.J. Withers et al., Nat. Rev. Methods Primers 1 (1) (2021) 18.
[24] J. Schindelin et al., Nat. Methods 9 (7) (2012) 676–682.
[25] M.J. Willemink et al., Eur. Radiol. 23 (2013) 1623–1631.
[26] G. Wang, J.C. Ye, B. De Man, Nat. Mach. Intell. 2 (12) (2020) 737–748.
[27] J.S. Jørgensen et al., Phil. Trans. r. Soc. A 379 (2204) (2021) 20200192.
[28] E. Papoutsellis et al., Phil. Trans. r. Soc. A 379 (2204) (2021) 20200193.
[29] T. Faragó et al., J. Synchrotron Radiat. 29 (3) (2022) 916–927.
[30] M. Beister, D. Kolditz, W.A. Kalender, Phys. Med. 28 (2) (2012) 94–108.
[31] J. Prakash, U. Agarwal, P.K. Yalavarthy, Sci. Rep. 11 (1) (2021) 1–9.
[32] A. Eklund et al., Med. Image Anal. 17 (8) (2013) 1073–1094.
[33] L. Helfen et al., Appl. Phys. Lett. 94 (10) (2009) 104103.
[34] S. Harasse, W. Yashiro, A. Momose, Opt. Express 19 (17) (2011) 16560–16573.
[35] L. Sun et al., Meas. Sci. Technol. 32 (4) (2021) 045403.
[36] E.A. Starke Jr, J.T. Staley, Prog. Aerosp. Sci. 32 (2–3) (1996) 131–172.
[37] X. Zhang, Y. Chen, J. Hu, Prog. Aerosp. Sci. 97 (2018) 22–34.
[38] P.J. Withers, M. Preuss, Annu. Rev. Mater. Res. 42 (2012) 81–103.
[39] S. Wu, T. Xiao, P. Withers, Eng. Fract. Mech. 182 (2017) 127–156.
[40] H. Villarraga-Gómez, Quality Magazine 55 (6) (2016) 20–23.
[41] A. Thompson, I. Maskery, R.K. Leach, Meas. Sci. Technol. 27 (7) (2016) 072001.
[42] P.J. Withers, M. Preuss, Annu. Rev. Mater. Res. 42 (1) (2012) 81–103.
[43] L. Babout, E. Maire, R. Fougeres, Acta Mater. 52 (8) (2004) 2475–2487.
[44] E. Maire et al., Acta Mater. 56 (18) (2008) 4954–4964.
[45] T. Ueda, L. Helfen, T.F. Morgeneyer, Acta Mater. 78 (2014) 254–270.
[46] O. Furukimi et al., ISIJ Int. (2018) . ISIJINT-2017-609.
[47] K. Watanabe et al., Tetsu-to-Hagane/j. Iron Steel Instit. Jpn. 104 (2) (2018) 65–71.
[48] T. Tancogne-Dejean et al., Acta Mater. 205 (2021) 116556.
[49] P.-O. Bouchard, et al., Numerical modeling of ductile fracture at the microscale combined with X-Ray laminography and digital volume correlation, in: AIP Conference Proceedings, AIP Publishing LLC, 2017.
[50] K.K. Chawla, Composite Materials: Science and Engineering, Springer Science & Business Media, 2012.
[51] P. Mangalgiri, Bull. Mater. Sci. 22 (3) (1999) 657–664.
[52] C. Bouvet, S. Rivallant, J.-J. Barrau, Compos. Sci. Technol. 72 (16) (2012) 1977–1988.
[53] P. Wright et al., J. Compos. Mater. 42 (19) (2008) 1993–2002.
[54] A. Scott et al., Compos. Sci. Technol. 71 (12) (2011) 1471–1477.
[55] S. Stock, Int. Mater. Rev. 53 (3) (2008) 129–181.
[56] D. Bull et al., Compos. A Appl. Sci. Manuf. 52 (2013) 62–69.
[57] F. Xu et al., J. Synchrotron Radiat. 17 (2) (2010) 222–226.
[58] H. Deyhle et al., NDT and E Int. 111 (2020) 102222.
[59] G. Borstnar et al., Compos. A Appl. Sci. Manuf. 71 (2015) 176–183.
[60] D. Bull et al., Compos. Sci. Technol. 75 (2013) 55–61.
[61] P. Verboven et al., Plant J. 81 (1) (2015) 169–182.
[62] Q.T. Ho et al., Plant Cell Environ. 39 (1) (2016) 50–61.
[63] S. Harasse, W. Yashiro, A. Momose, *X-ray phase laminography with a grating interferometer using iterative reconstruction*, *AIP Conference Proceedings*, American Institute of Physics, 2012.
[64] G.-A. Nazri, G. Pistoia, Lithium Batteries: Science and Technology, Springer Science & Business Media, 2008.
[65] S.C. Singhal, K. Kendall, High-Temperature Solid Oxide Fuel Cells: Fundamentals, Design and Applications, Elsevier, 2003.
[66] J. Deng et al., Joule 4 (3) (2020) 511–515.
[67] J.O. Majasan et al., J. Phys.: Energy 3 (3) (2021) 032011.
[68] Y. Xie et al., J. Power Sources 542 (2022) 231753.
[69] P. Pietsch, V. Wood, Annu. Rev. Mat. Res. 47 (2017) 451–479.
[70] R. Moroni et al., Sci. Rep. 6 (1) (2016) 30109.
[71] J. Gelb et al., J. Power Sources 357 (2017) 77–86.
[72] C. Tan et al., Cell Rep. Phys. Sci. 2 (12) (2021) 100647.
[73] H.C. Parks et al., J. Mater. Chem. A 11 (39) (2023) 21322–21332.
[74] X. Lu et al., Nat. Commun. 11 (1) (2020) 1–13.

[75] W. Du et al., Small Methods 5 (5) (2021) 2001193.
[76] W. Du et al., J. Power Sources 520 (2022) 230818.
[77] N. Shateri et al., Batteries Supercaps (2022) e202200035.
[78] C. Rahe et al., J. Power Sources 433 (2019) 126631.
[79] A. Fordham et al., Joule 7 (11) (2023) 2622–2652.
[80] P. Gajjar, IPC Quick Start Guide: IPC programming for Inspect-X, 2017.
[81] B. Hu et al., Joule 8 (9) (2024) 2623–2638.
[82] S. Hao et al., Nano Energy 82 (2021) 105744.
[83] J. Bailey et al., J. Microsc. 267 (3) (2017) 384–396.
[84] J. Chen et al., Nat. Commun. 15 (1) (2024) 10811.
[85] P.R. Shearing, Nat. Energy 1 (11) (2016) 1–2.
[86] V. Wood, Nat. Rev. Mater. 3 (9) (2018) 293–295.
[87] M. Loveridge, M. Dowson, Why Batteries Fail and How to Improve Them: Understanding Degradation to Advance Lithium-Ion Battery Performance, Warwick Manufacturing Group, University of Warwick, The Faraday Institution, 2021.
[88] T. Burnett, P. Withers, Nat. Mater. 18 (10) (2019) 1041–1049.
[89] X. Zhang et al., Adv. Energy Mater. 11 (2) (2021) 2000808.
[90] M. Daly et al., Acta Mater. 130 (2017) 56–68.
[91] J. Scharf et al., Nat. Nanotechnol. 17 (5) (2022) 446–459.
[92] F. Cognigni et al., ChemElectroChem 10 (7) (2023) e202201081.
[93] M.D. Kok et al., Sustain. Energy Fuels 3 (11) (2019) 2972–2976.
[94] T.M. Heenan et al., Adv. Energy Mater. 10 (47) (2020) 2002655.
[95] Y.-S. Yu et al., Nat. Commun. 9 (1) (2018) 1–7.
[96] S. Müller et al., Adv. Energy Mater. 10 (28) (2020) 1904119.
[97] K. Witte et al., Nano Lett. 20 (2) (2020) 1305–1314.
[98] C. Tan et al., Materials 11 (11) (2018) 2157.
[99] H.-Y. Nguyen, Computed tomography for the non-destructive imaging of cultural heritage: X-ray, Gamma and Neutron sources, Thesis Submitted to the Department of Art in Conformity with the . . ., 2011.
[100] N. Rudolph-Mohr et al., Plant and Soil 469 (2021) 489–501.
[101] R.F. Ziesche et al., Nat. Commun. 11 (1) (2020) 777.
[102] F. Salvemini et al., Anal. Methods 7 (1) (2015) 271–278.
[103] X. Gao et al., Joule 6 (3) (2022) 636–646.
[104] T. Burnett et al., Sci. Rep. 4 (1) (2014) 1–6.
[105] F. Cianciosi, et al., BM18, the New ESRF-EBS Beamline for Hierarchical Phase-Contrast Tomography, in: 11th Mechanical Engineering Design of Synchrotron Radiation Equipment and Instrumentation (MEDSI'20), Chicago, IL, USA, 24–29 July 2021, JACOW Publishing, Geneva, Switzerland, 2021.
[106] C. Walsh et al., Nat. Methods 18 (12) (2021) 1532–1541.
[107] M. Hurst, et al., Hierarchical X-ray laminography for the observation of in situ processes in large, application relevant samples, in: 14th International Conference on Synchrotron Instrumentation (SRI), 2022.
[108] D. Vavrik et al., Case Stud. Nondestr. Test. Eval. 6 (2016) 47–55.
[109] D. Ou et al., J. Instrum. 14 (02) (2019) P02018.
[110] S. Legrand et al., Heritage Science 2 (2014) 1–11.
[111] B. Cai et al., Acta Mater. 117 (2016) 160–169.
[112] F. García-Moreno et al., Adv. Mater. 33 (45) (2021) 2104659.
[113] C. Tan et al., ACS Appl. Energy Mater. 1 (9) (2018) 5090–5100.
[114] D.P. Finegan et al., Nat. Commun. 6 (1) (2015) 1–10.
[115] M. Sharp et al., J. Electrochem. Soc. 169 (2) (2022) 020526.
[116] M. Yokota et al., Powder Technol. 380 (2021) 265–272.
[117] T. Saida et al., Angew. Chem. Int. Ed. 51 (41) (2012) 10311–10314.
[118] Y. Ozaki et al., Powder Metall. 62 (2) (2019) 146–154.
[119] P. Raimondi, Synchrotron Radiat. News 29 (6) (2016) 8–15.
[120] H. Xu et al., Adv. Energy Mater. 11 (19) (2021) 2003908.
[121] D.P. Finegan et al., ACS Energy Lett. 7 (12) (2022) 4368–4378.
[122] G.-X. Zhang et al., Cell Rep. Phys. Sci. (2022) 101008.
[123] J. Solomon et al., Med. Phys. 47 (9) (2020) 3961–3971.
[124] J. Park et al., Phys. Med. Biol. 63 (14) (2018) 145011.
[125] Z. Pan et al., IEEE Access 7 (2019) 36322–36333.
[126] S. Müller et al., Nat. Commun. 12 (1) (2021) 1–12.
[127] K. Tang et al., Comput. Chem. Eng. 161 (2022) 107768.
[128] Z. Jiang et al., Nat. Commun. 11 (1) (2020) 1–9.
[129] E. Liotti et al., Sci. Adv. 4 (4) (2018) eaar4004.
[130] S.R. Daemi et al., Small Methods 6 (10) (2022) 2200887.
[131] S. Minaee et al., IEEE Trans. Pattern Anal. Mach. Intell. (2021) .